ISSN 1674-1056
http://cpb.iphy.ac.cn
http://iopscience.iop.org/cpb
中国物理 B
Chinese Physics
中国物理 Chinese Physics B

Dynamics of an ultrasound contrast agent microbubble near spherical boundary in ultrasound field

Ji-Wen Hu(胡继文)[1,2], Lian-Mei Wang(王练妹)[1], Sheng-You Qian(钱盛友)[2], Wen-Yi Liu(刘文一)[1], Ya-Tao Liu(刘亚涛)[1], Wei-Rui Lei(雷卫瑞)[1]

Citation: Chin. Phys. B . 2019, 28(11): 114301 . **doi:** 10.1088/1674-1056/ab4d3f
Journal homepage: http://cpb.iphy.ac.cn; http://iopscience.iop.org/cpb

What follows is a list of articles you may be interested in

Interaction between encapsulated microbubbles: A finite element modelling study

Chen-Liang Cai(蔡晨亮), Jie Yu(于洁), Juan Tu(屠娟), Xia-Sheng Guo(郭霞生), Pin-Tong Huang(黄品同), Dong Zhang(章东)

Chin. Phys. B . 2018, 27(8): 084302 . **doi:** 10.1088/1674-1056/27/8/084302

Influence of mode conversions in the skull on transcranial focused ultrasound and temperature fields utilizing the wave field separation method: A numerical study

Xiang-Da Wang(王祥达), Wei-Jun Lin(林伟军), Chang Su(苏畅), Xiu-Ming Wang(王秀明)

Chin. Phys. B . 2018, 27(2): 024302 . **doi:** 10.1088/1674-1056/27/2/024302

Theoretical analysis of interaction between a particle and an oscillating bubble driven by ultrasound waves in liquid

Yao-Rong Wu(武耀蓉), Cheng-Hui Wang(王成会)

Chin. Phys. B . 2017, 26(11): 114303 . **doi:** 10.1088/1674-1056/26/11/114303

Adaptive optimization on ultrasonic transmission tomography-based temperature image for biomedical treatment

Yun-Hao Zhu(朱昀浩), Jie Yuan(袁杰), Stephen Z Pinter, Oliver D Kripfgans, Qian Cheng(程茜), Xue-Ding Wang(王学鼎), Chao Tao(陶超), Xiao-Jun Liu(刘晓峻), Guan Xu(徐冠), Paul L Carson

Chin. Phys. B . 2017, 26(6): 064301 . **doi:** 10.1088/1674-1056/26/6/064301

Impact of cavitation on lesion formation induced by high intensity focused ultrasound

Pengfei Fan(范鹏飞), Jie Yu(于洁), Xin Yang(杨鑫), Juan Tu(屠娟), Xiasheng Guo(郭霞生), Pintong Huang(黄品同), Dong Zhang(章东)

Chin. Phys. B . 2017, 26(5): 054301 . **doi:** 10.1088/1674-1056/26/5/054301

Dynamics of an ultrasound contrast agent microbubble near spherical boundary in ultrasound field*

Ji-Wen Hu(胡继文)[1,2], Lian-Mei Wang(王练妹)[1], Sheng-You Qian(钱盛友)[2,†], Wen-Yi Liu(刘文一)[1], Ya-Tao Liu(刘亚涛)[1], and Wei-Rui Lei(雷卫瑞)[1]

[1] School of Mathematics and Physics, University of South China, Hengyang 421001, China
[2] School of Physics and Electronics, Hunan Normal University, Changsha 410081, China

(Received 27 August 2019; revised manuscript received 29 September 2019; published online 23 October 2019)

The goal of this article is to establish the conditions of excitation where one has to deal with ultrasound contrast agent (UCA) microbubbles pulsating near biological tissues with spherical boundary in ultrasound field for targeted drug delivery and cavitation-enhanced thrombolysis, etc., and contributes to understanding of mechanisms at play in such an interaction. A modified model is presented for describing microbubble dynamics near a spherical boundary (including convex boundary and concave boundary) with an arbitrary-sized aperture angle. The novelty of the model is such that an oscillating microbubble is influenced by an additional pressure produced by the sound reflection from the boundary wall. It is found that the amplitude of microbubble oscillation is positively correlated to the curve radius of the wall and negatively correlated to the aperture angle of the wall and the sound reflection coefficient. Moreover, the natural frequency of the microbubble oscillation for such a compliable wall increases with the wall compliance, but decreases with the reduction of the wall size, indicating distinct increase of the natural frequency compared to a common rigid wall. The proposed model may allow obtaining accurate information on the radiation force and signals that may be used to advantage in related as drug delivery and contrast agent imaging.

Keywords: ultrasound contrast agent (UCA) microbubble, spherical boundary, ultrasound, natural frequency

PACS: 43.25.+y, 43.80.+p, 02.90.+p **DOI:** 10.1088/1674-1056/ab4d3f

1. Introduction

Research of acoustical response of ultrasound contrast agent (UCA) microbubbles has attracted wide interests from both the medical and acoustical communities, not only for providing a better understanding of their complex dynamics, but also for their potential use for targeted drug delivery and molecular imaging.[1–3] Apart from these medical applications, UCA microbubble sonication is being recently utilized in several other medical areas, such as thrombus dissolution, gas embolotherapy, sonoporation, and micro-pumping.[4–6] In each case, it requires consistent mathematical and physical knowledge of sonicated microbubble oscillation near different types of boundaries.

Some experimental studies[7–9] have investigated microbubble dynamics in confined spaces and have shown that the proximity of a boundary can produce considerable changes in the oscillation amplitude of a microbubble and its scattered echo.[10,11] Moreover, there are some results indicating that microbubble collapse is mitigated as the driving frequency increases, or the microbubble is closer to the rigid boundary.[12] Theoretical attempts to model microbubble sonication in a confined configuration usually utilizes the boundary integral method,[11] finite element method[13] or method of images,[14,15] which describes the nonlinear oscillations of a microbubble near rigid boundaries and on the effects of boundaries such as a single wall, two parallel walls, or a tube, and so on. Most investigations focused on a cavitation microbubble occurring near a flat boundary. In fact, microbubble cavitation in a curved boundary is not uncommon in human body tissues. It is well known that red blood cells, which contain large amount of concave shape and are approximately 7.5–8.7 μm in diameter[16] whereas the mean diameter of UCA microbubbles is generally less than 5 μm.[17] Medical imaging shows the growing atherosclerotic plaque is ellipsoid or spherical in shape,[18] and there are a lot of irregular filling cavities in the clot aggregated by platelets and red blood cells crowded.[19,20] Cavitation microbubbles often create many cavities or pits on the surface of the target object during the removal of kidney and bladder stones with focusing of the shockwave.[21] In addition, microbubble forms a jet directed toward the interface due to interaction of cavitation microbubbles with cell membranes and produces a porous wall during sonoporation,[22] which potentially has a significant impact on membrane permeation observed in the experiment.[23] Accordingly, it is imperative to understand the bubble dynamics in soft tissues with curved boundaries or cavities for such as targeted drug delivery,[24] and so on.

A number of studies have been dedicated to the microbub-

*Project supported by the National Natural Science Foundation of China (Grant Nos. 11774088 and 11474090), the Hunan-Provincial Natural Science Foundation of China (Grant No. 13JJ3076), and the Science Research Program of Education Department of Hunan Province of China (Grant No. 14A127).
†Corresponding author. E-mail: syqian@foxmail.com
© 2019 Chinese Physical Society and IOP Publishing Ltd

ble dynamics near a curved boundary. For example, Tomita *et al.*[25,26] generated a laser-induced microbubble near a curved rigid boundary and the experiments present that the velocity of the micro jet increases while the shape of the rigid boundary changes from concave into convex. Wu *et al.*[27] reported an experimental study of microbubble dynamics near a convex free surface and focus on the strength of the micro jet when microbubble collapses. Obreschkow *et al.*[28] studies the behavior of a bubble in a droplet in micro gravity. They observed two liquid jets escaping from the drop when the microbubble collapses, and a shorter microbubble life time in the droplet than the microbubble in an infinite fluid. Also, the spike and the splash on the concave free surface are not as violent as a flat free surface.

However, the microbubble dynamics near a spherical boundary with arbitrary-sized aperture angle has received less attention, and the influence of the geometric parameters of the boundary remains poorly understood to date. In this paper, we assume that an oscillating microbubble is influenced by additional pressure come from sound reflections on a wall.[29] The sound reflection combining with the image method are employed to demonstrate the microbubble confinement near the wall. Considering that UCA-type microbubbles have immediate biomedical applications such as the delivery of drugs and the instigation of sonoporation, the geometric setups and parameters are chosen to be of relevance for intravascular microbubble dynamics in medicine. This article focuses on the influences of the concave wall sizes and the wall properties, and specially studies the natural frequency responses of wall properties, and finally summarizes our results.

2. Theory

Suppose a spatially uniform ultrasound pressure field: the ultrasound wave length is of the order of 1 mm and thus much larger than the dimension of the region of interest surrounding a UCA microbubble.[30] The microbubble retains a spherical shape throughout the simulation for low expansion ratio.[31]

We further assume that the fluid surrounding the microbubble is incompressible, and the liquid flow is irrotational. The velocity potential φ, fluid velocity v and acoustic pressure p obey the equation of continuity and are written in terms of a scalar velocity potential as[32]

$$v = -\nabla\varphi, \tag{1}$$

$$p = -\mathrm{i}\omega\rho\varphi, \tag{2}$$

$$(\nabla^2 + k^2)\varphi = 0, \tag{3}$$

where k is the wave number for a pressure wave of angular frequency ω, and ρ is the liquid density. The symbol i denotes the unit imaginary number. From Eqs. (3) and (3) it is easy arrived at

$$\nabla^2 p + k^2 p = 0. \tag{4}$$

When a microbubble oscillates near a concave wall in an ultrasound field as shown in Fig. 1, equation (4) may be expressed as

$$\nabla^2 p + k^2 p = -4\pi(q + q'). \tag{5}$$

Equation (5) can be understood as a source equation in the acoustic field. In this equation, q and q' represent the point source produced by a microbubble oscillation and its reflection source by a concave wall, respectively. Using Green's second identity, $G(\boldsymbol{r}, r')$, the acoustic pressure p in liquid is given as

$$p(\boldsymbol{r}) = \int_{s_b} \left[G(\boldsymbol{r}, \boldsymbol{r}')\frac{\partial p}{\partial n} - p\frac{\partial G(\boldsymbol{r}, \boldsymbol{r}')}{\partial n} \right] \mathrm{d}s' + \int_{V'} q(r')G(\boldsymbol{r}, \boldsymbol{r}')\mathrm{d}v' + \int_{V''} q'(r'')G(\boldsymbol{r}, r'')\mathrm{d}v''. \tag{6}$$

It means that in Eq. (6) the total pressure p includes three sound sources, that is,

$$p(\boldsymbol{r}) = p_{\mathrm{i}}(\boldsymbol{r}) + p_{\mathrm{s}}(\boldsymbol{r}) + p_{\mathrm{r}}(\boldsymbol{r}). \tag{7}$$

In Eq. (7), p_{i} is the driving pressure source term. The second term p_{s} and the third term p_{r} on the right hand side of the equation represents the scattered pressure and reflected pressure, respectively.

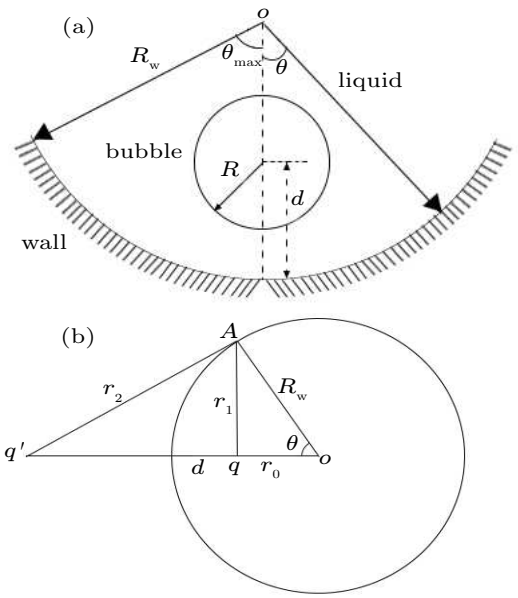


Fig. 1. Schematic sketch of a contrast agent microbubble near a concave wall (a) and its mirror images (b). Here d is the distance between the center of the microbubble and the wall, R_{w} is the curvature radius of the wall, and $\theta_{\max}$ is the aperture angle of the wall.

To describe the confinement effect on the microbubble oscillation, the concave wall is replaced by an identical image bubble oscillating in-phase with a real microbubble and positioned at the mirrored image point. The dynamics of the real microbubble is influenced by the pressure emitted by the image microbubble or by the wall. To this end, suppose that a point source q located at distance r from the center, inside the

sphere, has an image q' at distance r' from the center. The point source q, its image, and the center of the sphere lie on a straight line, as is the script on the left-hand side of Fig. 1. On the interface, the continuity of potential field at any point A on the sphere yields the value

$$q' = -\frac{R_{\rm w}}{r_0}q. \tag{8}$$

The total potential inside the cavity is expressed as

$$\phi_{\rm in} = \frac{q}{4\pi\varepsilon r_1} - \frac{q'}{4\pi\varepsilon r_2}, \tag{9}$$

where ε is the media coefficient, r_1 and r_2 are the distances. The induced source density at any point A on the sphere can be obtained by taking the derivative of the potential $\phi_{\rm in}$,

$$\sigma_{\rm in} = \varepsilon\Big(-\frac{\partial\phi_{\rm in}}{\partial r}\Big)\Big|_{r=R_{\rm w}} = -\frac{q}{4\pi R_{\rm w}^2}\frac{R_{\rm w}^2 - r_0^2}{(R_{\rm w}^2 + r_0^2 - 2R_{\rm w}r_0\cos\theta)^{3/2}}, \tag{10}$$

where θ $(0 \leqslant \theta \leqslant \pi)$ is the usual polar angle between the z-axis. If we introduce $\delta = r_0/R_{\rm w} = 1 - d/R_{\rm w}$, the surface charge density may be written concisely as

$$\sigma_{\rm in} = -\frac{q}{4\pi R_{\rm w}^2}\frac{(1-\delta^2)}{(1+\delta^2 - 2\delta\cos(\theta))^{3/2}}. \tag{11}$$

Notice that the absolute value of $\sigma_{\rm in}$ is largest in the direction of the closest point for $\theta = 0$ and is smallest in the opposite direction for $\theta = \pi$. The solution of the "inverse" problem which is a point source outside of a sphere is the same as the roles of the real source and the image source reversed. The only change necessary is the surface source density, where the normal derivative is now outward, implying a source of sign. In general, the induced source of the eccentric vibration of a microbubble confined to a concave wall with aperture angle $\theta_{\max}$ as shown in Fig. 1 may be obtained by

$$\begin{aligned} q' &= \iint_S \sigma_{\rm in}{\rm d}S = \int_0^{\theta_{\max}} \sigma_{\rm in} 2\pi R_{\rm w}^2 \sin\theta {\rm d}\theta \\ &= \Big[\frac{1-\delta^2}{2\delta\sqrt{1+\delta^2-2\delta\cos(\theta_{\max})}} - \frac{1+\delta}{2\delta}\Big]q. \end{aligned} \tag{12}$$

The induced source is $q' = -q$ as one integrates over the surface of sphere. Equation (12) shows that the induced source is affected by the aperture angle of $\theta_{\max}$. Theoretical and experimental studies show that microbubble dynamics near a curved boundary is strongly affected by the surrounding wall with curvature parameter ξ and the constraint coefficient with $F(\xi) = \xi^2/(1+\xi)$.[25,26] In the case of spherical boundary, we assume that the induced source is proportional to $\alpha\xi^2/(1+\xi)$, where α is the factor of proportionality. The constraint coefficient on microbubble vibration near the spherical boundary with $\theta_{\max}$ may now be expressed as

$$F(\xi,\theta_{\max}) = -\Big[\frac{1-\delta^2}{2\delta\sqrt{1+\delta^2-2\delta\cos(\theta_{\max})}} - \frac{1+\delta}{2\delta}\Big]\frac{\xi^2}{(1+\xi)}q. \tag{13}$$

The curvature parameter ξ satisfies $\xi = (\sqrt{d^2+4R_{\rm w}^2} \pm d)/2R_{\rm w}$ for a spherical boundary with curvature radius $R_{\rm w}$. The type of the spherical boundary is specified by the parameter ξ, giving convex spherical boundary for $-d$, concave spherical boundary for $+d$, and a flat boundary (i.e., $R_{\rm w} \to \infty$) when $\xi = 1$.

We assume that the boundary wall behaves as a point source with q' and both point-source microbubbles are equal, pulsating in phase. We substitute Eq. (12) into the third term of the right-hand side of Eq. (6) and compare with Eq. (7), one may found the following empirical formula for the reflected pressure,

$$p_{\rm r} = F(\xi,\theta_{\max})p_{\rm s}. \tag{14}$$

The scattered pressure from a real point source is expressed as

$$p_{\rm s} = \frac{\rho(R^2\ddot{R} + 2R\dot{R}^2)}{d}, \tag{15}$$

where R and $\dot{R}$ are the radius and radial velocity of microbubble, respectively. If the sound reflection coefficient at the liquid-wall boundary is taken into account, the reflected pressure may be written as

$$p_{\rm r} = Z_{\rm r}F(\xi,\theta_{\max})p_{\rm s}, \tag{16}$$

where $Z_{\rm r}$ represents the acoustic reflection coefficient of the liquid-wall boundary and is defined as[29]

$$\begin{array}{ll} 0 < Z_{\rm r} < 1, & \text{rigid wall,} \\ Z_{\rm r} = 0, & \text{no wall,} \\ -1 < Z_{\rm r} < 0, & \text{compliable wall.} \end{array} \tag{17}$$

The limiting values of reflection coefficient $Z_{\rm r} \approx 1$ and $Z_{\rm r} \approx -1$ correspond to absolutely rigid or compliant interface conditions, respectively.[33]

The dynamics of a UCA microbubble in a spherical boundary may be described using a modified Rayleigh–Plesset equation[34] that accounts for the reflected pressure.

$$R\ddot{R} + \frac{3}{2}\dot{R}^2 = \frac{\Delta P}{\rho}, \tag{18}$$

with

$$\begin{aligned} \Delta P = &\Big(P_0 + \frac{2\sigma}{R_0} - P_v\Big)\Big(\frac{R_0}{R}\Big)^{3\gamma} + P_v - P_0 - \frac{2\sigma}{R} - \frac{4\mu\dot{R}}{R} \\ &- \frac{4k_s\dot{R}}{R^2} - 4\chi\Big(\frac{1}{R_0} - \frac{1}{R}\Big) - p(t) - p_{\rm r}, \end{aligned}$$

where μ is the dynamic viscosity of the liquid, γ is the polytropic exponent, P_0 is the ambient pressure and $p(t)$ is the driving pressure pulse. P_v is the vapor pressure, k_s is the microbubble's shell viscosity and χ is the shell elasticity, σ is the surface tension, and R_0 is the initial radius.

Assuming that the pulsation amplitude is small, namely, $R(t) = R_0(1+x(t))$, where $|x(t)| \ll 1$, we can obtain the natural frequency of a UCA microbubble near a sphere wall,

$$\omega_0^2 = \frac{3\gamma P_0 + 2(3\gamma-1)\sigma/R_0 + 4\chi/R_0}{\rho_L R_0^2 \alpha} = \frac{\omega_\infty^2}{\alpha}, \tag{19}$$

where ω_∞ denotes the nature frequency in an unbounded fluid, and α is

$$\alpha = 1 + \frac{R_0 F(\xi, \theta_{\max})}{d}. \tag{20}$$

The parameters are taken from the literature:[11] $\mu = 0.02$ Pa·s, $\gamma = 1.07$, $P_0 = 1.013 \times 10^5$ Pa, $P_v = 2330$ Pa, $k_s = 0.72 \times 10^{-8}$ kg/s, $\chi = 0.51$ N/m, $\sigma = 0.072$ N/m. In the following, we show simulated solutions to Eqs. (16) and (19) using the parameters mentioned above.

3. Results and discussion

We first validate our model by comparing to the estimates of other investigators. When taking no account of translational microbubble motion, a comparison of the influence of the curved surface of two models, i.e., Eq. (13) and a model with the constraint coefficient $F(\xi) = \xi^2/(1+\xi)$ given by Tomita *et al.* for the aperture angle of $\theta_{\max} = \pi/2$. We plot in Fig. 2 four values of the maximum microbubble radius/initial microbubble ratio with the curvature radius R_w. For four curvature radius $R_w = 1.5R_0$, $3.5R_0$, $7.0R_0$ and $70R_0$, the corresponding values of the curvature parameters ξ are 1.5584, 1.1694, 1.0817 and 1.0079 for concave sphere surface, and 0.6417, 0.8551, 0.9245 and 0.9922 for convex sphere surface, respectively. It is seen that the ratio of $R_{\max}/R_0$ decreases with increasing the curvature radius R_w in the case of convex surface for the two models. Conversely, the ratio increases with R_w for concave surface. The change of the maximum radius with curvature radius ($\delta R_{\max}/\delta R_w$) in our model is larger than that of Tomita *et al.* for microbubble near a convex boundary, which is comparable with the microbubble behavior near a concave boundary.[25,26] These can be explained from the enclosed degree of the curved boundary with characteristics parameter ξ and the sphere radius R_w. For example, the pressure of the reflected wave from the curved boundary (non-sphere boundary) with $\xi = 1.1694$ is more stronger than that from the concave sphere boundary with $R_w = 3.5R_0$ since the free-space volume occupied by of a microbubble vibrating in a concave sphere boundary is larger than that of a concave curved boundary for $\theta_{\max} = \pi/2$. We can see $F(\xi, \theta_{\max}) > 1$ with $f(\xi) > 1$ for concave boundary and $F(\xi, \theta_{\max}) < 1$ with $f(\xi) < 1$ for convex boundary, and the $R_{\max}/R_0$ will go to a fixed value, i.e. $1.26R_0$, as the radius of curvature approaches infinity for both boundaries. This result is consistent with reports that a concave curved surface shows higher compression on microbubble oscillation than that of a convex curved surface under the same condition.[25,26]

We next consider the correlation between constraint coefficient and aperture angle. We simulated Eq. (13) for obtaining a solution trajectory which tends toward a stable equilibrium point as seen in Fig. 3, where the constraint coefficient is plotted against the aperture angle $\theta_{\max}$ for different values of the curvature radius R_w. When R_w is small, the level of the constraint coefficient keeps at a very low level, which means a weak suppression to bubble oscillation. This is the situation that the curvature radius is very small. Reflection of sound waves off of surfaces is affected by the shape of the surface. When the curvature radius are too small, often only a small proportion of the wave is reflected and have a less compression on microbubble oscillation. Conversely, a convex sphere boundary with large curvature radius R_w has a large constraint coefficient and produces relatively large suppression to oscillating microbubble accordingly. It is noted that the constraint coefficient can quickly reach a stable value when $R_w = 70R_0$ with a smaller value of $\theta_{\max}$. The analysis confirms the validity of the present model of the spherical boundary.

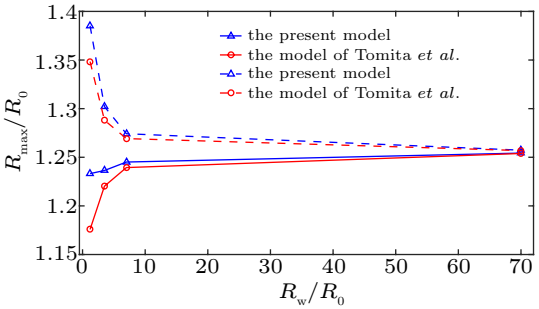


Fig. 2. The ratio of $R_{\max}/R_0$ as a function of the ratio of R_w/R_0 for two different boundaries for a microbubble at the distance of $d = 1.1R_0$. The broken curves represent convex boundary and the solid curves represent concave boundary.

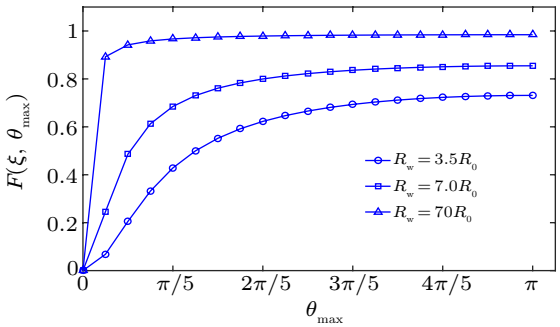


Fig. 3. Comparison of the constraint coefficient at different $\theta_{\max}$ for a microbubble at the distance of $d = 1.1R_0$ near the convex spherical surface.

We further explored in detail the natural frequency of oscillation of a UCA microbubble confined in a concave sphere wall. Wall rigidity, microbubble size and microbubble position are taken into account for evaluating the effects on the natural frequency of a UCA microbubble oscillation. Figure 4 illustrates the natural frequency of a microbubble increases gradually with the radius of curvature of the concave wall for an absolute rigid wall ($Z_r = 1$). It means that the natural frequency

of the microbubble in the corresponding unbounded field is the upper limit of that in the rigid wall. For the same concave wall, a smaller microbubble has a larger natural frequency. The change in frequency with concave wall size ($\delta f/\delta R_{\rm w}$) is larger for a smaller microbubble. For example, in a 5 μm radius concave wall, $\delta f/\delta R_{\rm w} = 0.1217$ MHz/μm for a microbubble radius of 1.5 μm and $\delta f/\delta R_{\rm w} = 0.0095$ MHz/μm for a microbubble radius of 2.45 μm. In ultrasound-assisted drug delivery, drug extravasation through the blood vessel wall is usually observed in small blood vessels with diameters less than 20 μm in vivo experiments.[35] This change is also observed in vessels in theoretical calculations.[36] Unlike the case of a rigid wall, the natural frequency of a microbubble oscillation decreases with reducing the radius at the vicinity of a compliable wall ($Z_{\rm r} = -0.3$), and is much larger than that of a rigid wall for the same microbubble and wall size.

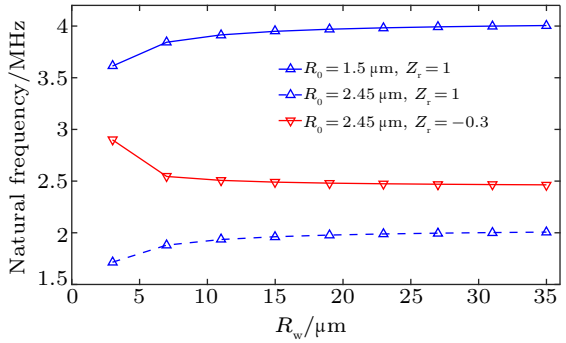


Fig. 4. The microbubble natural frequency as a function of microbubble radius for the microbubble lying near concave wall at the distance of $d = 1.1R_0$ and $\theta_{\rm max} = \pi$.

Figure 5 shows the microbubble natural frequency as a function of aperture angle of concave wall for two different types of walls when a UCA microbubble is closed to the concave wall. For the case of rigid wall ($Z_{\rm r} = 0.6$), the microbubble natural frequency decreases from 2.28 MHz to 1.96 MHz with $\theta_{\rm max}$ ranging from $\pi/10$ to π. However, the natural frequency in the vicinity of a compliable wall ($Z_{\rm r} = -0.6$) increases from 2.38 MHz to 3.02 MHz for the same microbubble and $\theta_{\rm max}$. Thus it can be seen that the two different types of boundaries have noticeable effects on the natural frequency of a microbubble oscillation.

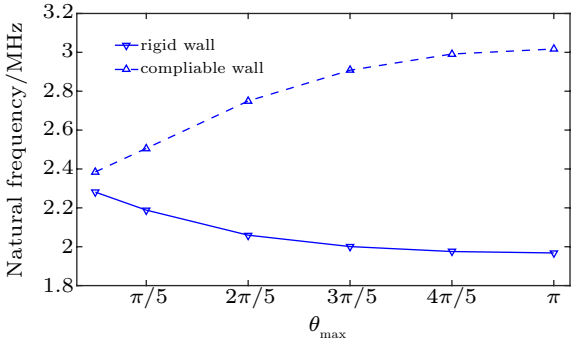


Fig. 5. The microbubble natural frequency as a function of aperture angle of a concave wall for two different types of walls as the microbubble lying near the concave wall at the distance of $d = 1.1R_0$ and $R_{\rm w} = 5$ μm.

In the above simulation results the microbubble natural frequency is susceptible to the type of concave wall. Equations (19) and (20) are employed to further study the natural frequency of microbubble oscillation influenced by wall properties. Figure 6 shows that the natural frequency of a microbubble with initial radius of 2.45 μm near a rigidity wall with $R_{\rm w} = 5$ μm and $\theta_{\rm max} = \pi/2$ decreases with increasing $Z_{\rm r}$. The microbubble frequency approaches the value in an absolute rigidity wall as the stiffness increases, which is significantly lower than that in the unbounded field and in the normal tissue. When a tumor develops further and $Z_{\rm r}$ stiffness increases, the frequency further decreases to 1.88 MHz. Conversely, the microbubble natural frequency increases with increasing the absolute value of $-Z_{\rm r}$ when a microbubble vibrates in the vicinity of a compliable concave wall. The change in frequency with absolute value of reflection coefficient $|Z_{\rm r}|$ ($\delta f/\delta|Z_{\rm r}|$) is larger than that of in the rigidity case. For example, in an absolute value of $Z_{\rm r} = |-0.3|$, $\delta f/\delta Z_{\rm r} = 1.29$ MHz for a compliance wall and $\delta f/\delta Z_{\rm r} = 0.65$ MHz for the case of rigidity wall for a microbubble radius of 2.45 μm. The same change is also found in blood vessels as reported in the literature.[30,36] It is apparent that in stiffer walls the microbubble natural frequency (where the maximum bubble expansion is reached) is higher. The shift towards higher frequencies with wall stiffness was also reported by Martynov *et al.*[37] This could be explained from the mass and spring perspective where more rigid wall has larger stiffness and therefore larger nature frequencies.

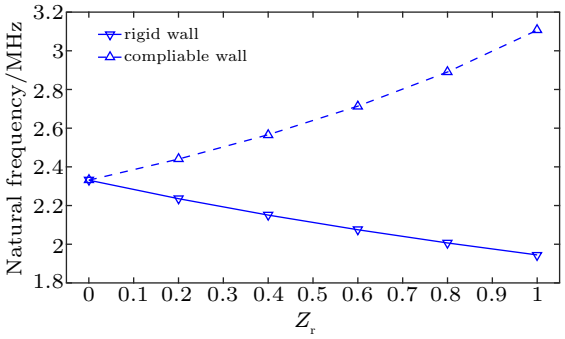


Fig. 6. The microbubble natural frequency as a function of reflection coefficient for two different types of walls with $d = 1.1R_0$, $Rw = 5$ μm and $\theta_{\rm max} = \pi/2$.

4. Conclusion

We have presented a model to study a UCA microbubble response confined in a spherical boundary. The present model can be used not only for the dynamic behavior of a microbubble confined in concave sphere boundary but also for demonstrating the microbubble constraint near convex sphere boundary. The influence of an additional pressure on microbubble can be demonstrated by the reflected pressure from wall surface. Two kinds of boundaries for a concave wall have been considered, i.e. a rigid wall and a compliable wall, which may

correspond to the vasculature of a developing tumor. Numerical results demonstrate that the natural frequency of mircobubble in a rigid wall is smaller compared to that in unbounded field, and further decreases with the reducing concave size. Interestingly, this frequency increases with the decreasing concave wall size. Moreover, the natural frequency of microbubble in the unbounded field is the lower limit of the bubble natural frequency in a compliable wall and the upper limit in an absolute rigid wall. For medical applications, the changes of the frequency spectrum of the microbubble show the changes of the material property including concave wall size and its compliance.

References

[1] Qin S, Caskey C F and Ferrara K W 2009 *Phys. Med. Biol.* **54** R27
[2] Yildiz Y O, Eckersley R J, Senior R, Lim A K, Cosgrove D and Tang M X 2015 *Ultrasound Med. Biol.* **41** 1938
[3] Teng X D, Guo X S, Tu J and Zhang D 2016 *Chin. Phys. B* **25** 124314
[4] Delalande A, Leduc C, Midoux P, Postema M and Pichon C 2015 *Ultrasound Med. Biol.* **41** 1913
[5] Sheeran P S, Matsuura N, Borden M A, Williams R, Matsunaga T O, Burns P N and Dayton P A 2016 *IEEE Trans. Ultrason Ferroelectr. Freq. Control.* **64** 252
[6] Tang M, Loo J F, Wang Y, Zhang X, Kwok H C, Hui M, Leung C C, Kong S K, Wang G and Ho H P 2017 *Lab Chip* **17** 474
[7] Zhong P, Zhou Y and Zhu S 2001 *Ultrasound Med. Biol.* **27** 119
[8] Garbin V, Cojoc D, Ferrari E, Di Fabrizio E, Overvelde M L J, van der Meer S M, de Jong N, Lohse D and Versluis M 2007 *Appl. Phys. Lett.* **90** 114103
[9] Wong Z Z, Kripfgans O D, Qamar A, Fowlkes J B and Bull J L 2011 *Soft Matter* **7** 4009
[10] Zhao Z F, Zhang W J, Niu L L, Meng L and Zheng H R 2018 *Acta Phys. Sin.* **67** 194320 (in Chinese)
[11] Doinikov A A, Aired L and Bouakaz A 2011 *Phys. Med. Biol.* **56** 6951
[12] Miao H, Gracewski S M and Dalecki D 2008 *J. Acoust. Soc. Am.* **124** 2374
[13] Cai C L, Yu J, Tu J, Guo X S, Huang P T and Zhang D 2018 *Chin. Phys. B* **27** 084302
[14] Wang Q, Manmi K and Calvisi M L 2015 *Phys. Fluids* **27** 022104
[15] Wang L, Tu J, Guo X S, Xu D and Zhang D 2014 *Chin. Phys. B* **23** 124302
[16] Diez-Silva M, Dao M, Han J, Lim C T and Suresh S 2010 *MRS Bull.* **35** 382
[17] Park D, Song G, Jo Y, Won J and Son T 2016 *Plos One* **11** e0157707
[18] Epah J, Pálfi K, Dienst F L, Malacarne P F and Bremer R 2018 *Theranostics* **8** 2117
[19] Kallmes D F and Fujiwara N H 2016 *Am. J. Neuroradiol* **2 3** 1580
[20] Cines D B, Lebedeva T, Nagaswami C, Hayes V, Massefski W, Litvinov R I, Rauova L, Lowery T J and Weisel J W 2014 *Blood* **123** 1596
[21] Johnsen E and Colonius T 2008 *J. Acoust. Soc. Am.* **124** 2011
[22] Curtiss G A, Leppinen D M, Wang Q X and Blake J R 2013 *J. Fluid. Mech.* **730** 245
[23] Vogel A, Schweiger P, Frieser A, Asiyo M N and Birngruber R 1990 *J. Quant. Electron.* **26** 2240
[24] Sutton J T, Ivancevich N M, Perrin S R, Vela D C, Holl and C K 1994 *Phys. Med. Biol.* **39** 813
[25] Tomita Y and Shima A 1986 *J. Fluid. Mech.* **169** 535
[26] TomitaY, Robinson P B, Tong R P and Blake J R 2002 *J. Fluid. Mech.* **466** 259
[27] Wu S J, Zuo Z G, Ren Z B and Liu S H 2018 *Proc. 10th International Symposium on Cavitation*, May 14–16, 2018, Maryland, USA p. 308
[28] Obreschkow D, Kobel P, Dorsaz N, de Bosset A, Nicollier C and Farhat M 2006 *Phys. Rev. Lett.* **97** 094502
[29] Hu J W, Qian S Y, Sun J N, Lv Y B and Hu P 2015 *Chin. Phys. B* **24** 094301
[30] Qin S and Ferrara K W 2006 *Phys. Med. Biol.* **51** 5065
[31] Stride E and Saffari N 2003 *Proc. Inst. Mech. Eng. H.* **217** 429
[32] Morse P M and Ingard K U 1968 *Theoretical Acoustics* (New York: McGraw Hill)
[33] Hasheminejad S M 2001 *Acustica* **87** 443
[34] van der Meer S M, Dollet B, Voormolen M M, Chin C T, Bouakaz A, de Jong N, Versluis M and Lohse D 2007 *J. Acoust. Soc. Am.* **121** 648
[35] Stieger S M, Caskey C F, Adamson R H, Qin S, Curry F R, Wisner E R and Ferrara K W 2007 *Radiology* **243** 112
[36] Qin S and Ferrara K W 2007 *Ultrasound Med. Biol.* **33** 1140
[37] Martynov S, Stride E and Saffari N 2009 *J. Acoust. Soc. Am.* **126** 2963